THE ASTROPHYSICAL JOURNAL, 461:L83–L86, 1996 April 20

UNLENSING MULTIPLE ARCS IN 0024+1654: RECONSTRUCTION OF THE SOURCE IMAGE

WESLEY N. COLLEY,[1,2] J. ANTHONY TYSON,[3] AND EDWIN L. TURNER[2]
wes@astro.princeton.edu, tyson@physics.att.com, elt@astro.princeton.edu
Received 1995 December 15; accepted 1996 February 8

ABSTRACT

A unique reconstruction of the image of a high-redshift source galaxy responsible for multiple long arcs in the $z = 0.4$ cluster 0024+1654 is obtained by inverse lensing. Deep *B*- and *I*-band imaging with the *Hubble Space Telescope* enables high resolution of the arcs due to strong gravitational lensing of the background source. The gravitational lens in the foreground cluster is thus used to obtain a magnified view of the distant source. Four strongly lensed images of the source lead to a unique reconstruction. Each of the long arcs, when unlensed, leads to the same reconstructed source image, exhibiting a beaded, ringlike morphology. The *U* luminosity of the ring alone is equivalent to that of a normal galaxy. This is likely a galaxy in formation.

Subject headings: cosmology: observations — galaxies: clusters: individual (Cl 0024+1654) — galaxies: formation — gravitational lensing — methods: observational

1. INTRODUCTION

Strong gravitational lensing can in principle provide unprecedented views of distant background sources (Zwicky 1937; see Blandford & Narayan 1992 for a review). This can lead to a unique reconstruction of the source image, given enough information in the lensed image; generally, this works only if there are multiple images of the source. For example, Kochanek & Narayan (1992) obtained a full inversion of a lensed radio source in both intensity and polarization, the full Einstein ring providing the needed constraints. Since the discovery of strongly lensed long "arcs" around massive clusters of galaxies (Soucail, Fort, & Picat 1987; Lynds & Petrosian 1986), it has been hoped that such highly stretched images of background galaxies could be used to obtain at least a one-dimensional improvement of resolution of the source galaxy. Indeed, several long arcs seen in ground-based imaging show structure along the arc. The 0.″1 resolution of the *Hubble Space Telescope* (*HST*), combined with the magnification by the gravitational lens, can yield enhanced resolution in the source plane.[4]

The reconstructed source image is however only as accurate as the lens model. Thus, one concern has been whether such a reconstruction is unique. This is particularly worrisome in cases in which there are few constraints on the detailed lens model, as in single long arcs. The multiple long arcs in the $z = 0.39$ cluster 0024+1654 present an opportunity to break lens model degeneracies and develop a unique reconstruction of the source. These relatively bright multiple arcs (redshifts unknown; see § 4) in 0024+1654 were discovered by Koo (1988) photographically, and various lens models based on deeper ground-based CCD imaging of these arcs have been advanced (Kassiola, Kovner, & Fort 1992; Wallington, Kochanek, & Koo 1995). Deep imaging suggests at least three and perhaps four strongly lensed images of the same blue source. These models, however, were based on the assumption of only three source images and/or an incomplete search of the source plane.

Five arcs, images of the same blue source galaxy, are clearly seen in the *HST* imaging (see below). The same detailed morphology is seen in each arc, but flipped by the lens. Thus it is possible to sufficiently constrain a full lens model in which the parameters for the dark matter lens and cluster galaxy lenses are all allowed to vary. In this Letter, we present a fully two-dimensional reconstruction with 100 pc resolution for the high-redshift source of the major arcs seen in the distant, massive cluster 0024+1654.

2. OBSERVATIONS AND DATA REDUCTION

The data were taken on 1994 October 14 UT in three visits of two orbits each, plus one additional orbit. The total integration time was 15,000 s. We obtained three series of orbits in each of two filters: F450W (blue) and F814W (red). The 1100 s exposures were offset by ~10″, which enabled us to fill in the gaps between the Wide-Field and Planetary Camera 2 (WFCP2) chips effectively. Deep-imaging data over a larger field from the Kitt Peak 4 m telescope were used to define the large-scale mass distribution, as described below.

We made multiple passes over the data, using an initial, cleaned co-addition of all the data as support for bad-pixel removal. After cosmic-ray detection and removal using STSDAS CRREJ, we co-added the data for each of the three orbital series. Each of the three stacks represents seven images, 8400 s total, in blue and six images, 6600 s total, in red. We then registered the images for each chip from the three orbital series and obtained their mean, excluding areas with no data. This process yielded a stacked image of the three runs, most of which contained the full signal from all three runs. Next we performed a final cleaning of the six images (three chips, two bands), using DAOFIND and IMCLEAN to find and remove bad or hot pixels.

We then mosaicked the three chips (again employing IRAF GEOTRAN for registration) to obtain a continuous image in the familiar "L" configuration of WFC2 measuring 2.′7 on a side. After sky-subtracting and calibrating the blue and red

[1] Supported by the Fannie and John Hertz Foundation, Livermore, CA 94551.
[2] Department of Astrophysical Sciences, Princeton University, Princeton, NJ 08544.
[3] Bell Laboratories, Lucent Technologies, 600 Mountain Avenue, Murray Hill, NJ 07974.
[4] Based on observations with the NASA/ESA *Hubble Space Telescope*, obtained at the Space Telescope Science Institute, which is operated by AURA, Inc., under NASA contract NAS5-26555.

images, we produced a third, intermediate band by mean-averaging the blue- and red-band images. These three RGB images, converted to stretched 8 bit log intensity, were then packed into a 3 × 8 bit color TIFF image, shown in Figure 1 (Plate L15).

Figure 2 (Plate L16) is a stretched monochrome reproduction of part of the blue image and shows our naming convention for the five arcs. Note in the color WFPC2 image shown in Figure 1 that arcs A, B, and C as well as a counterarc D and a demagnified subimage E can be identified by their identical morphology, blue color, and surface brightness (preserved by lensing). Lensed images at these positions were also found in experiments by forward ray-tracing a single diffuse source through a complete lens model, to be described elsewhere.

3. SOURCE RECONSTRUCTION

The WFPC2 image in Figure 1 shows that the arcs are well resolved in these images, revealing at least five separate features in the common source. Arcs A, C, and D are highly magnified, and we concentrate on producing a self-consistent source-image reconstruction from these three arcs. We also use the location and orientation of arcs B and E to constrain our multiple-lens parameter-space search. Our procedure for image reconstruction is somewhat different than that usually followed in lens modeling. Rather than seeking a unique lens model, we instead make use of the multiple images to arrive at a self-consistent source-image reconstruction by varying the parameters of the multiple lenses. Some lens parameters are separately constrained by the known locations of cluster galaxies and from arclet data over wider field deep ground-based imaging.

3.1. *Lens Model*

Our goal is to place the reconstructions of arcs A, C, and D at the same point in the source plane, produce the correct image parity, and generate identical orientation and dimension in all three reconstructions. All lenses in the cluster are modeled as soft-core isothermal distributions (Grossman & Narayan 1988), but with an outer mass cutoff, which yields (for the spherical case) a deflection angle

$$\frac{\alpha}{\alpha_0} = \begin{cases} \dfrac{r}{r_{\rm core}}\left(0.75 - \dfrac{r^2}{8r_{\rm core}^2}\right), & r < r_{\rm core}, \\ \dfrac{5r_{\rm core}}{8r} + \dfrac{\beta r_{\rm out}}{r}\left(\arctan\dfrac{r}{r_{\rm out}} - \arctan\dfrac{r_{\rm core}}{r_{\rm out}}\right), & r \geq r_{\rm core}, \end{cases}$$

where $\alpha_0 = 4\pi\sigma_v^2/c^2$, the deflection angle for an isothermal distribution, $r_{\rm core}$ is the soft-core radius, $r_{\rm out}$ is the outer mass cutoff, and $\beta = (1 + r_{\rm core}^2/r_{\rm out}^2)$. We further generalize each lens to be elliptical.

The lenses consist of the massive dark matter lens and the many cluster galaxies. The parameters for each lens are its location on the sky, its effective velocity dispersion, ellipticity, orientation, and outer cutoff. Dressler & Gunn (1992) studied this cluster and listed photometry and redshifts for many of the brighter cluster galaxies. We computed approximate Faber-Jackson (F-J) masses for 48 of the brighter lens galaxies based on aperture photometry. The positions of the cluster galaxies are fixed by their observed red centroids, and the orientation of their mass ellipticity is set at the observed isophote orientation. Rough starting values for their velocity dispersions are obtained from the F-J relation, after *K*-correction, using the observed 814 nm (760 nm in cluster rest frame) magnitudes and $B - I$ and $R - I$ colors: $\log \sigma_v = 4.3 - R/10$ ($h = 0.7$).

3.2. *UNLENS*

The starting parameters for the main dark matter lens were obtained from weak-lens inversion of 1200 arclets, *not* the strongly lensed arcs, from deep wide-field 4 m imaging (described elsewhere). Rather than forward ray-trace a model source image, we developed code to backward ray-trace the observed arcs to the source. First, a mapping from the image plane to the source plane is created by vector addition of the pretabulated radial distortions of the lens components. The mapping may contain caustics and other abrupt features, which could compromise resolution in the source plane with inadequate sampling. We therefore dynamically subsample the image plane with small triangles, which map into triangles on the lens plane, regardless of distortions or inversions. Since disparate portions of the image plane arrive on each source-plane pixel, we divide each pixel value by the number of image-plane pixels mapped into it. To speed calculation, we only map image-plane pixels above a particular threshold.

We found results from this scheme to agree with an equivalent but independent code we have also developed, called UNLENS (Tyson et al. 1996). This code uses multiple-ray pixel subsampling of the image plane, rather than polygon filling, to generate the source image with smaller pixels but is otherwise algorithmically similar to the first.

3.3. *Optimization*

Since these lens masses are approximate and do not account for some of the halo dark matter in each cluster galaxy, we varied the outer cutoff of some of the galaxy masses, particularly those projected near any of the arcs. Our goodness-of-fit criterion is based on an optimal match for the reconstructions of arcs A, C, and D in the source plane. Since we have 49 lenses in our model, with six parameters each, we could have spent a great deal of time searching through the available 294-dimensional space to optimize our results. Instead, we initially tried to optimize our reconstructions as a function of the location, velocity dispersion, and ellipticity and orientation of the central dark potential, keeping the cluster galaxy mass parameters fixed at their F-J values. The normalization absorbs our ignorance of the distance to the source. We found that the reconstructed position in the source plane of different arcs depends strongly and *differently* on the lens parameters of the main potential as well as several individual cluster galaxy parameters.

Figure 3 illustrates our method. We select the three prominent features seen in all three arcs (see Fig. 1) and follow these features through the lens back to the source plane for each arc. In each of Figures 3*a*–3*d*, we plot two graphs: the lower shows the trajectory of the reconstructed source features in the source plane (1 pixel = 0.″025) while the upper plot gives the rms error in reconstructed source-image positions in the source plane as a function of the parameter varied: main potential *x*- or *y*-position in the image plane (1 pixel = 0.″1), main potential velocity dispersion, or main potential ellipticity. Figure 3*a* shows the trajectories of these features in the reconstructed source as they respond to movement of the main potential centroid along *x*. Similarly, Figures 3*b*–3*d* show those trajectories in response to movement of the main potential in

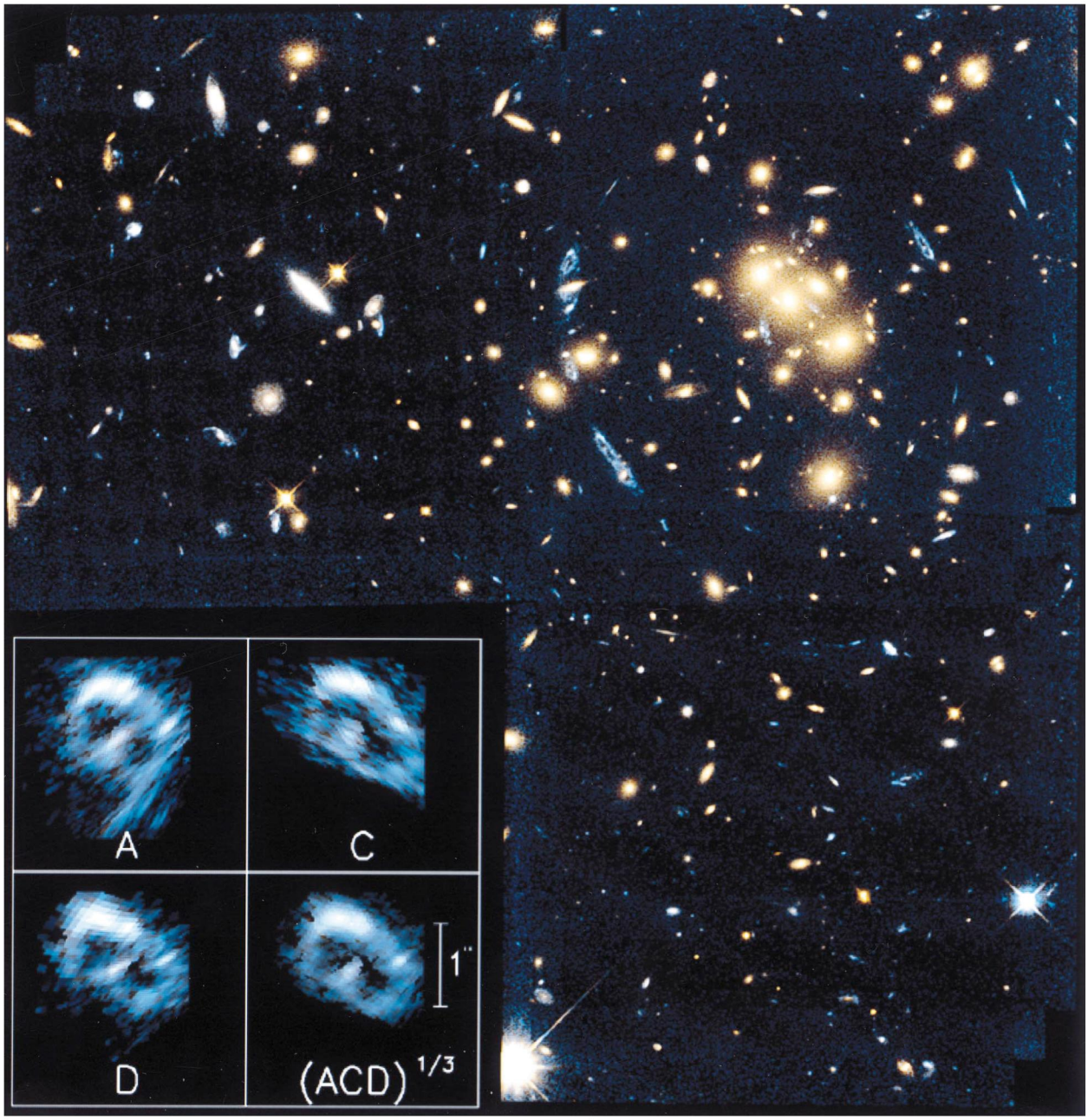

FIG. 1.—Color image of the field of the massive $z = 0.39$ cluster 0024+1654 generated from co-added 15,000 s imaging data in the F450W and F814W filters on the *HST* WFC2 chips. North is up and east is left. The longest side of the image is 2.′7. Five blue arcs, each an image of the same background source at much higher redshift, may be seen. Three of them, two arcs to the southeast and one counterarc to the northwest, are highly magnified. Our reconstruction of the source (see text) by unlensing each of these longest arcs is shown in the inset. The source-plane scale is indicated by a 1″ bar. Note that the resolution is greater along the long axis of the arcs.

COLLEY, TYSON, & TURNER (see 461, L84)

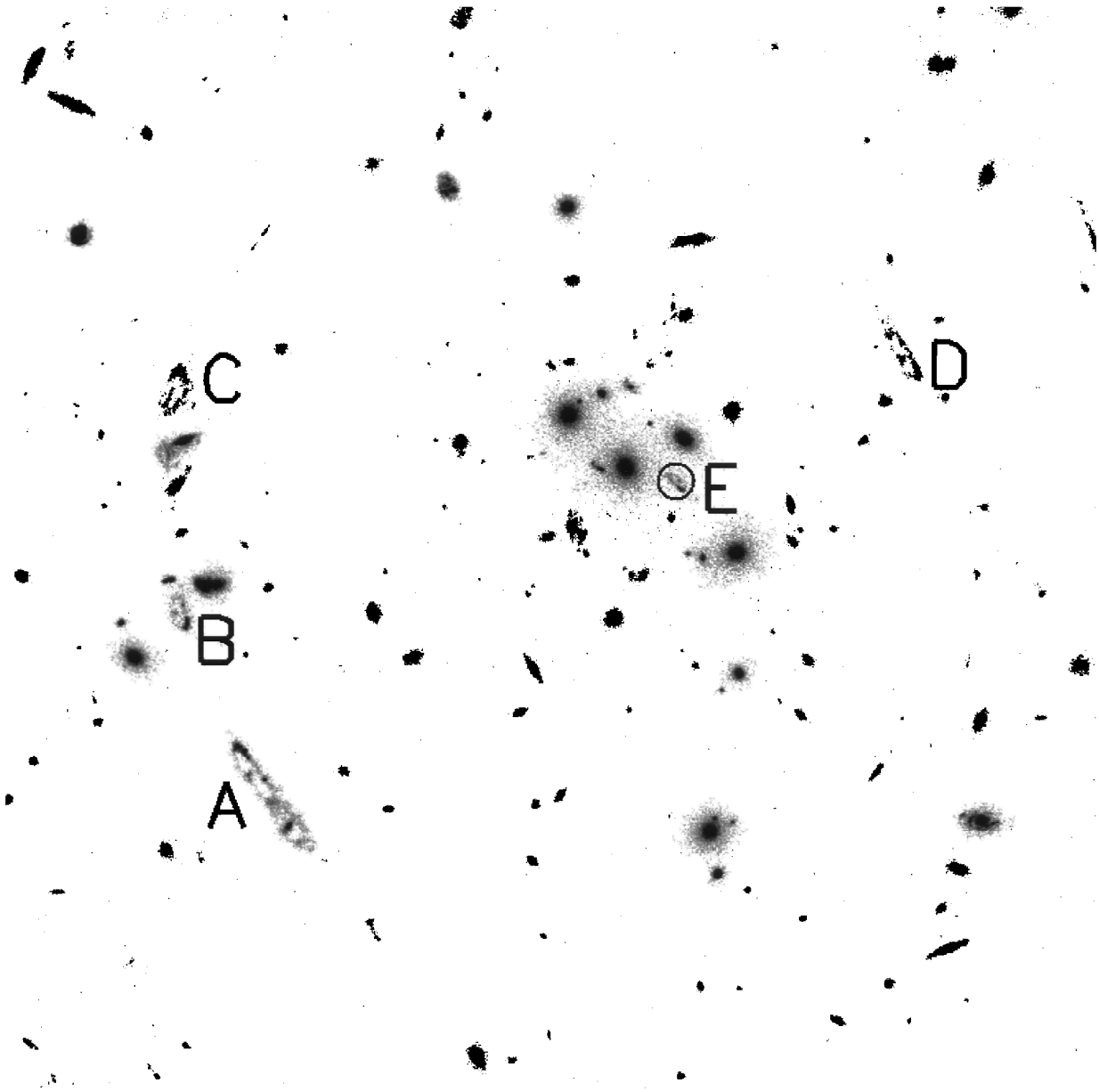

FIG. 2.—Nomenclature for arcs A, B, C, D, and E marked on a stretched monochrome subfield extracted from the blue WFC2 image. The existence of image E constrains the soft core of the main potential.

COLLEY, TYSON, & TURNER (see 461, L84)

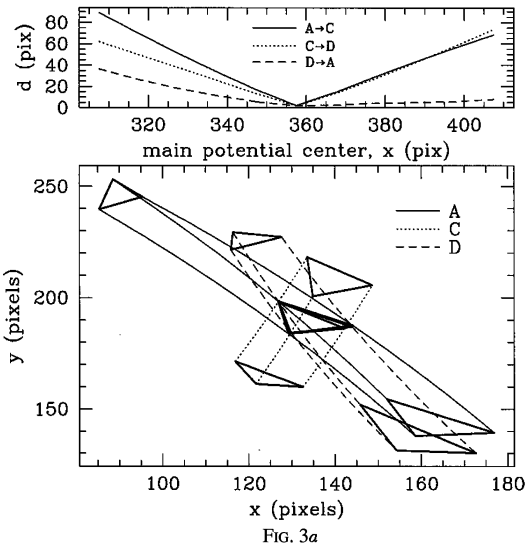

FIG. 3a

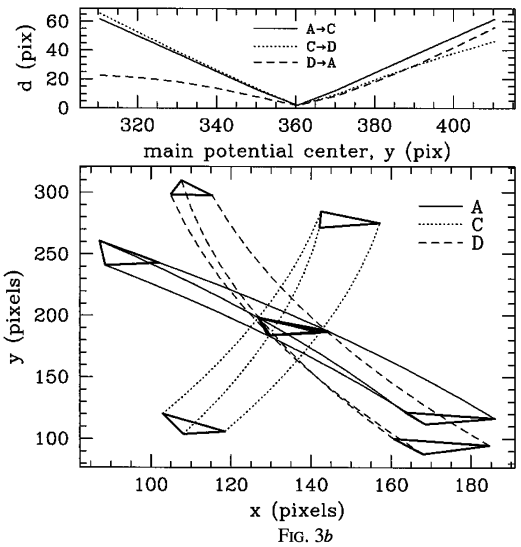

FIG. 3b

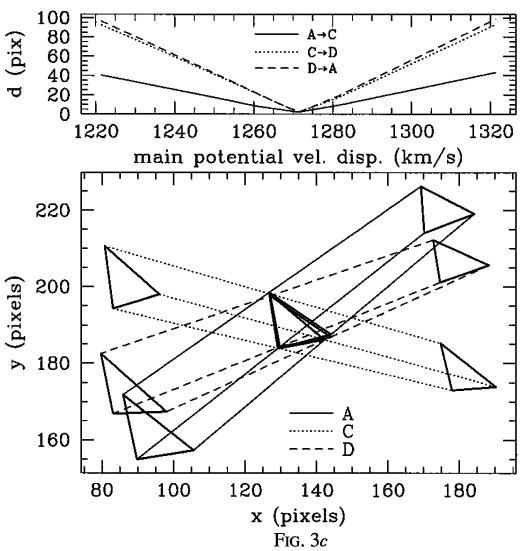

FIG. 3c

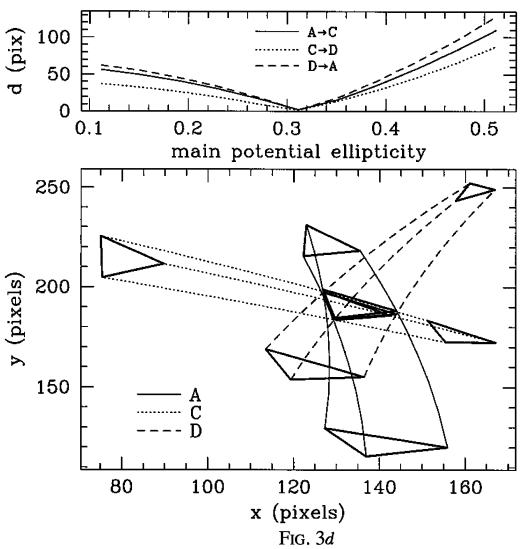

FIG. 3d

FIG. 3.—(*a*) *Bottom*: Trajectories in the source plane of bright features in the reconstructed source image, parameterized in the *x*-position of the main potential, for arcs A, C, and D (see text). One pixel is 0".025. *Top*: The rms distance between these "central" features in the source plane for each of the three reconstructed images. (*b–d*) Same as (*a*), but varying the *y*-position of the main potential, the velocity dispersion of the main potential, and the eccentricity of the main potential, respectively. Orientation was obtained by inversion of 1200 weak lensing arclets in the deep 4 m data.

y, variation of its velocity dispersion, and variation of the ellipticity of the main dark matter potential, respectively.

The "optimal" fit is given as the three roughly overlapping triangles near the center. Radiating from each triangle are the tracks followed by each of the triangles responding to the variable in question. The tracks extend to arbitrary endpoints, which are denoted again by heavy triangles. A global mix of these rms differences is what we want to minimize in order to reach self-consistency in the source reconstruction. We found that six cluster galaxies that are projected near the arcs influence the shape of the reconstructed source for that arc. We varied the lens parameters for these six galaxies from the starting F-J values to improve the match between the reconstructed images for arcs A, C, and D using the squared difference of their images as an error criterion. This procedure was repeated recursively, taking various routes through the lenses, to arrive at a global optimization.

3.4. *Source Image*

Our reconstructions of the source image corresponding to arcs A, C, and D are shown in the lower left corner of Figure 1. These color images were generated as described in § 2. In each image, the image-plane WFPC2 pixelization is visible and distorted in a different way for each of the three images, as expected. However, the main features of the source appear to have been produced self-consistently in each plot. Both the noise and artifacts are damped when the images are combined, as shown in the last of the four reconstructed source images in Figure 1. The similarity of the co-added image and the reconstructions gives us some confidence in the reconstruction.

Rather than summing the three reconstructed arcs, we may demand complete morphological consistency by instead combining them nonlinearly so that pixels must be maximally

consistent over the three reconstructed images. The harmonic mean of the three reconstructed source images is shown in the lower right panel of the inset in Figure 1, and a low pixel reject co-addition is shown in monochrome in Figure 4*a* (Plate L86). In Figures 4*b* and 4*c*, we show for comparison rotated and magnified images of arcs B and E. Note the morphological similarity between unreconstructed arcs B and E and the reconstructed source image from arcs A, C, and D. We did not unlens arcs B and E here, because of the extreme sensitivity to the mass distribution of the nearby galaxies. This will be discussed elsewhere.

4. ANALYSIS OF THE SOURCE

The reconstructed source resembles a blue "theta" or "B" of size 1″. With its beaded, ringlike nature, the source galaxy does not lie along the Hubble sequence. Moreover, it is large by comparison to most faint blue galaxies found in the *HST* Medium Deep Survey (Im et al. 1995). Most galaxies this bright with redshifts over $z = 1$ have angular diameters ~2 times smaller (Mutz et al. 1994). However, if the source were farther away, the $(1 + z)^4$ dimming would render all but the bright knots invisible and thus artificially reduce the apparent size. The source likely lies at a redshift between 1.2 and 1.8, since no emission line has been seen in deep spectroscopy. With a corresponding angular diameter distance of 860–890 h^{-1} Mpc, 1″ subtends 4.3 h^{-1} kpc of diameter.

Over this source redshift range, the F450W filter corresponds to 160–205 nm in the source rest frame and the F814W filter moves to 290–370 nm (*U* band) in the source rest frame. This systematic change in morphology from "normal" to "disturbed" seen in *HST* deep-imaging surveys is correlated with redshift, with most of the disturbed galaxies at redshifts greater than 1 (Forbes et al. 1995; Schade et al. 1995); we see these distant galaxies at UV wavelengths, highlighting lumpy regions of high star formation. The source's very blue color, transformed to the rest frame, is similar to that found for rapid star-forming galaxies (Bruzual & Charlot 1993).

It is interesting to speculate on the origin of the dark core inside the ring and the feature near the center. A very dusty protogalaxy could have this appearance; one would then be seeing UV from circumnuclear star-forming knots on the outskirts of the dust. Recently, a nearby example of a beaded nuclear ring in a barred galaxy has been found in a galaxy undergoing rapid star formation (Buta, Purcell, & Cracker 1995); a 5 kpc diameter oval ring with bright knots is seen in Hα. Other examples of clumpy nuclear rings are known (Morgan 1958; Schommer et al. 1988; Wilson et al. 1991), and several have a nuclear bar. Such a nuclear bar may be visible in Figure 4.

Combining this photometry with the deep ground-based *BRIgri* photometry and calibrating on the *gri* system, the knots around the ring in the source galaxy have an effective $g - i$ color of -0.4 to 0.2—characteristic of the bluest galaxies known. The $B - R$ and $r - i$ colors are similar to the colors of the faint blue galaxy population. The central "bar" in the source has a $B - I$ color 0.7 mag redder than the mean color of three blue knots around the ring. This lends support to the dust hypothesis. Taking a nearby nuclear ring galaxy as an example (see Fig. 8 of Buta et al. 1995), over 3 mag of localized extinction at 200 nm would be required to absorb the light interior to 4 kpc. The peak in interstellar dust absorption at 220 nm leads to sufficient extinction to make the observed hole, given a UV color excess of 0.7 mag, if we assume a rather flat extinction curve (low R_λ), which is typical of dense molecular regions where the grain sizes are large. If primeval, this object may not yet have formed a normal disk or spheroid and may consist mainly of a high star formation rate ring. Any spheroid should become visible in the IR. Unlensing deep *JHK*-band imaging may place more stringent limits on any older population of stars; the $H - K$ break for the source is expected longward of 860 nm, predicting a relatively red $I - J$ color.

The reconstructed source has an unlensed apparent *i* magnitude of 23.7 mag, which is consistent statistically with $z > 1.2$ (Schade et al. 1995). For $z > 1.2$, its absolute *U* magnitude is brighter than -20 mag ($h = 0.7$) from the ring alone. Accounting for several magnitudes of nuclear extinction at 200 nm would lead to a luminous source in the IR. We find no evidence of any outer ring in the source galaxy. The compound microscope formed by the cluster lens and *HST* affords a rare view of a young, star-forming, high-redshift galaxy.

We thank Phil Fischer, Frank Valdes, and Rick Wenk for help debugging UNLENS and Greg Kochanski for discussions. We also thank Bruce Draine for his useful comments on dust absorption. W. N. C. is grateful for the support of the Hertz Foundation and also thanks the Department of Astronomy at the University of Virginia for its hospitality. This work was partially funded by NASA grant NAGW-2173.

REFERENCES

Blandford, R. D., & Narayan, R. 1992, ARA&A, 30, 311
Bruzual, A., G., & Charlot, S. 1993, ApJ, 405, 538
Buta, R., Purcell, G. B., & Crocker, D. A. 1995, AJ, 110, 1588
Dressler, A., & Gunn, J. E. 1992, ApJS, 78, 1
Forbes, D. A., Elson, R. A. W., Phillips, A. C., Illingworth, G. D., & Koo, D. C. 1994, ApJ, 437, L17
Grossman, S. A., & Narayan, R. 1988, ApJ, 324, L37
Im, M., Casertano, S., Griffiths, R. E., Ratnatunga, K. U., & Tyson, J. A. 1995, ApJ, 441, 494
Kassiola, A., Kovner, I., & Fort, B. 1992, ApJ, 400, 41
Kochanek, C. S., & Narayan, R. 1992, ApJ, 401, 461
Koo, D. C. 1988, in Large-Scale Motions in the Universe, ed. V. C. Rubin & G. V. Coyne (Princeton: Princeton Univ. Press), 513
Lynds, R., & Petrosian, V. 1986, BAAS, 18, 1014
Morgan, W. W. 1958, PASP, 70, 364
Mutz, S. B., et al. 1994, ApJ, 434, L55
Schade, D., Lilly, S. J., Crampton, D., Hammer, F., Le Fèvre, O., & Tresse, L. 1995, ApJ, 451, L1
Schommer, R. A., Caldwell, N., Wilson, A. S., Phillips, M. M., Williams, T. B., & Turtle, A. J. 1988, ApJ, 324, 154
Soucail, G., Fort, B., & Picat, J. P. 1987, A&A, 172, L14
Tyson, J. A., Dell'Antonio, I. P., Kochanski, G. P., Colley, W. N., & Turner, E. L. 1996, in preparation
Wallington, S., Kochanek, K. S., & Koo, D. C. 1995, ApJ, 448, 51
Wilson, A. S., Helfer, T. T., Haniff, C. A., & Ward, M. J. 1991, ApJ, 381, 79
Zwicky, F. 1937, Phys. Rev. Lett., 51, 290

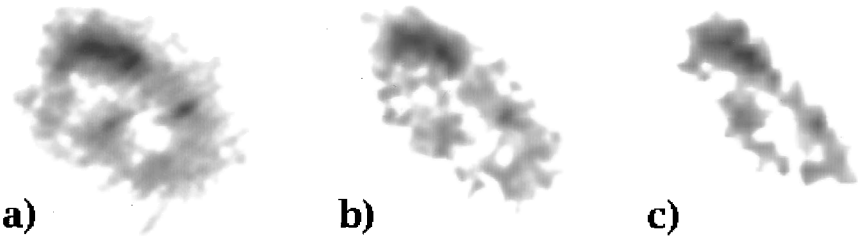

FIG. 4.—Reconstructed image of the source galaxy, based on maximum consistency (low pixel rejection). (*b*) Unreconstructed (image plane) image of arc B, rotated and magnified for comparison. (*c*) Unreconstructed image of arc E, rotated and magnified.

COLLEY, TYSON, & TURNER (see 461, L86)